ACS APPLIED MATERIALS & INTERFACES

Research Article

www.acsami.org

Synthesis of Au-Decorated V_2O_5@ZnO Heteronanostructures and Enhanced Plasmonic Photocatalytic Activity

Haihong Yin,[†,‡] Ke Yu,[*,†] Changqing Song,[†,‡] Rong Huang,[†] and Ziqiang Zhu[†]

[†]Key Laboratory of Polar Materials and Devices (Ministry of Education of China), Department of Electronic Engineering, East China Normal University, Shanghai 200241, P. R. China

[‡]School of Electronics and Information, Nantong University, Nantong 226019, China

Supporting Information

ABSTRACT: A ternary plasmonic photocatalyst consisting of Au-decorated V_2O_5@ZnO heteronanorods was successfully fabricated by an innovative four-step process: thermal evaporation of ZnO powders, CVD of intermediate on ZnO, solution deposition of Au NPs, and final thermal oxidization. SEM, TEM, EDX, XPS, and XRD analyses revealed that the interior cores and exterior shells of the as-prepared heteronanorods were single-crystal wurtzite-type ZnO and polycrystalline orthorhombic V_2O_5, respectively, with a large quantity of Au NPs inlaid in the V_2O_5 shell. The optical properties of the ternary photocatalyst were investigated in detail and compared with those of bare ZnO and V_2O_5@ZnO. UV–vis absorption spectra of ZnO, V_2O_5@ZnO, and Au-decorated V_2O_5@ZnO showed gradually enhanced absorption in the visible region. In addition, gradually decreased emission intensity was also observed in the photoluminescence (PL) spectra, revealing enhanced charge separation efficiency. Because of these excellent qualities, the photocatalytic behavior of the ternary photocatalyst was studied in the photodegradation of methylene blue under UV–vis irradiation, which showed an enhanced photodegradation rate nearly 7 times higher than that of bare ZnO and nearly 3 times higher than that of V_2O_5@ZnO, mainly owing to the enlarged light absorption region, the effective electron–hole separation at the V_2O_5–ZnO and V_2O_5–Au interfaces, and strong localization of plasmonic near-field effects.

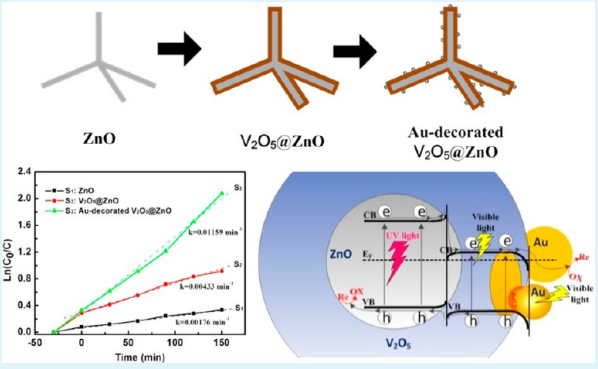

KEYWORDS: *heteronanostructures, photocatalysis, plasmonic properties, ZnO, V_2O_5*

INTRODUCTION

In recent years, semiconductor-based photocatalysis, as a kind of "green technology", has attracted considerable attention, because it represents an easy way to solve current energy and environmental problems through the use of solar light. Upon absorption of photons with energies greater than the band gap, electrons are excited from the valence band to the conduction band, creating electron–hole pairs. These charge carriers migrate to the surface to initiate reduction and oxidation reactions, through which organic contaminants in water and air are degraded. Up to now, varieties of semiconductors, such as metal oxides (TiO_2, ZnO, SnO_2, Fe_2O_3, and WO_3),[1−5] metal sulfurs (Cu_2S, CdS and ZnS),[6−8] and bismuth-based materials (BiOCl, BiOBr, and BiOI),[9−11] have been tested for the photocatalytic degradation of environmental pollutants. Among them, ZnO has been actively investigated as a photocatalyst because of the advantages of its high electron mobility, abundant morphologies, easy synthesis, and low cost.[12,13] However, the narrow light-responsive range and the high recombination rate are two fundamental issues hindering its large-scale application in industry.[13−15] The relatively wide band gap (3.3 eV) of ZnO means that electron–hole pairs can be generated only by ultraviolet radiation, which makes up only about 4% of the whole solar light spectrum.[16,17] Meanwhile, the high recombination rate (~90%) indicates that photogenerated electron–hole pairs can easily recombine before they move to the photocatalyst surface. To extend the light-absorption range and prolong the lifetimes of photoexcited charge carriers, various strategies have been developed, such as doping,[18,19] structure improvement,[20,21] and coupling with other components.[22−24]

Combining ZnO with other semiconductors having suitable band structures can enhance light absorption from the UV to the visible and near-infrared regions, induce the collection of the photogenerated electrons and holes on different semiconductor surfaces, and thus enhance the redox reactions of the electrons and holes. In this context, various ZnO-based photocatalysts such as TiO_2/ZnO,[25,26] CuO/ZnO,[23,27,28] SnO_2/ZnO,[14] and CdSe/ZnO[29] have been actively studied to improve their photocatalytic activities. In addition, the recently rapid development of surface plasmon resonance (SPR) has also offered a new route to overcome the limited efficiency of

Received: March 18, 2014
Accepted: August 20, 2014
Published: August 20, 2014

photocatalysts. Some nanoparticles (NPs) of noble metals, such as Au and Ag, have been introduced into ZnO nanostructures by a solution cogrowth or deposition−precipitation method, and improvements in photocatalytic activity were reported.[30−33] In these hybrid photocatalysts, the noble-metals NPs show strong absorption in the visible-light region due to surface plasmon resonance. Incorporating plasmonic noble-metal NPs into semiconductors can extend light absorption to longer wavelengths.[34−37] Moreover, using the solar radiation, the concentrated energy contained in localized plasmonic oscillations is transferred from the metal NPs (Au, Ag etc.) to the semiconductor, inducing the local generation of electron−hole pairs in the semiconductor. Therefore, the solar-energy-conversion efficiency should be improved, and an enhanced photocatalytic activity should be realized.

To collectively utilize the advantages of narrow-band-gap semiconductors and the SPR effects of noble-metal NPs, vanadium pentoxide (V_2O_5) and Au NPs were selected and coupled with wide-band-gap ZnO to improve its photocatalytic performance. V_2O_5, the most stable form of vanadium oxide, is widely used as an industrial catalyst. In the photocatalysis field, earlier studies revealed that the coupling of V_2O_5 with TiO_2 or SnO_2 is beneficial in improving photocatalysis efficiency.[16,38−41] However, the combination of V_2O_5 with ZnO for photocatalysis has rarely been investigated since first reported by Zou et al.[24] Because of the narrow band gap of V_2O_5 (2.2 eV), the combination of ZnO with V_2O_5 should be beneficial in extending light absorption from the UV to the visible region. Moreover, the introduced Au NPs can also promote the photocatalytic reaction because of SPR effects. In this work, a ternary plasmonic photocatalyst of Au-decorated V_2O_5@ZnO heteronanostructures was synthesized by a chemical vapor deposition (CVD) method combined with Au NP deposition and a thermal oxidization process. Generally, CVD is seldom used to synthesize V_2O_5-based nanostructures because of the relatively low melting temperature (685 °C) of V_2O_5. Herein, using the low sublimation temperature of the precursor $VO(acac)_2$ (acac = acetylacetonate), an intermediate of V_2O_5 was first deposited on single-crystal ZnO nanorods, forming initial intermediate heteronanostructures. After Au NP deposition and a thermal oxidization process at 350 °C, the final ternary photocatalyst of Au-decorated V_2O_5@ZnO nanostructures was successfully synthesized. Ultraviolet−visible (UV−vis) absorption measurements showed a significant red shift of the localized surface plasmon resonance (LSPR) peak and a marked enhancement of visible-light absorption in comparison with that of bare ZnO and V_2O_5@ZnO nanorods. The enhanced photocatalysis properties of the Au-decorated V_2O_5@ZnO nanostructures were also evaluated in terms of the degradation of methylene blue (MB), which is a cationic dye with the risk of causing burns to the eye, nausea, vomiting, and diarrhea.[42] Under the combined action of the Au NPs and the V_2O_5 shell, the as-prepared ternary photocatalyst showed a significantly enhanced photocatalytic activity, which could be ascribed to the extended light absorption, the effective transfer of photogenerated carriers, and the strong localization of plasmonic near-field effects.

EXPERIMENTAL SECTION

Synthesis of Au Nanoparticles. Au nanoparticles (NPs) were prepared according to the sodium citrate reduction method, in which distilled water was added to 0.1 g of $HAuCl_4$ to a total volume of 300 mL (0.001 mol/L). When this solution had been brought to a boil, 30 mL of sodium citrate solution (38.8 mmol/L) was rapidly added. After 15 min of continuous boiling, the color of the solution changed from pale yellow to dark red. After this mixture had cool in air to room temperature, the dark-red gold particles were collected and dispersed in 200 mL of distilled water to form a deep-red suspension.

Synthesis of ZnO Nanorods. The synthesis of ZnO nanorods was carried out in a horizontal quartz tube-furnace system at atmospheric pressure. Mixed ZnO (99.99% purity) and graphite (99.9% purity) powders were loaded in a quartz boat and placed at the center of the furnace. Then, the central temperature was increased to 720 °C at a rate of 15 °C min^{-1} and held for 60 min under a constant N_2 (99.9% purity) flow of 40 sccm. A cleaned silicon(100) substrate was placed ∼5 cm downstream of the source materials to collect the products (see Figure 1a). It should be noted that the source materials and the silicon substrate were placed in a small tube (inner diameter of about 6 cm) with one end open. After the furnace had cooled to room temperature, a light white layer was found to have deposited on the substrate.

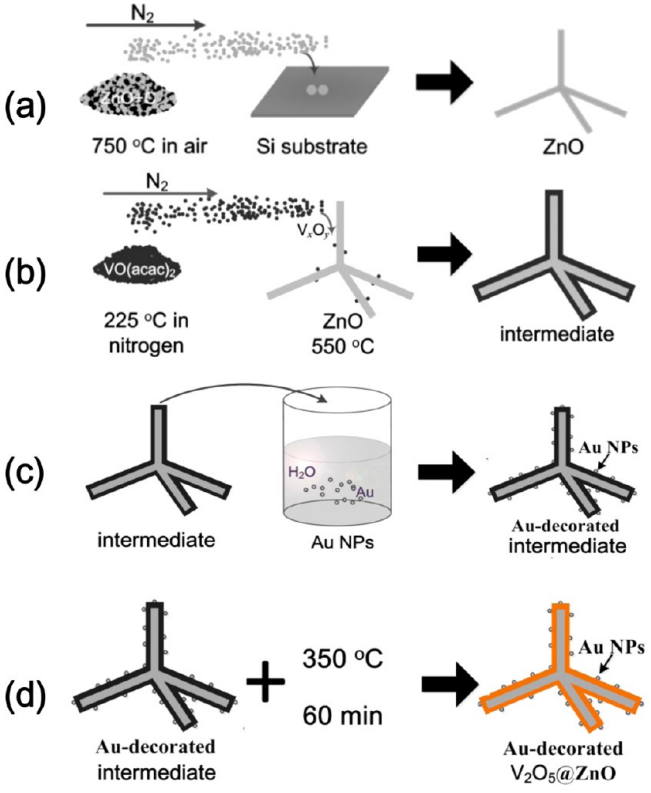

Figure 1. Schematic of the synthesis of Au-decorated V_2O_5@ZnO nanorods by a four-step process: (a) thermal evaporation growth of ZnO nanorods, (b) CVD of intermediate on ZnO nanorods, (c) solution deposition of Au NPs, and (d) final thermal oxidization at 350 °C.

Coating V_2O_5 on ZnO Nanorods and Decorating with Au Nanoparticles. V_2O_5 was coated on the ZnO nanorods using a gas-phase-based method. The CVD equipment was described in our previous studies,[43,44] and a schematic of this synthesis step is shown in Figure 1b. Vanadyl acetylacetonate [$VO(acac)_2$], whose sublimation temperature is 140−275 °C, was taken as the vanadium precursor and placed in a low-temperature zone where the temperature was controlled at 225 °C. The silicon substrate covered by ZnO nanorods was taken as the template and located at the tube center of the furnace. Before being heated, the furnace was pumped to expel oxygen in the tube, and pure nitrogen gas was introduced to reach atmospheric pressure. Then, the furnace was heated to 500 °C. A nitrogen flow (99.9% purity) at a constant rate of 50 sccm was used to carry the precursor vapor to the reaction furnace. After 40 min, all heating and

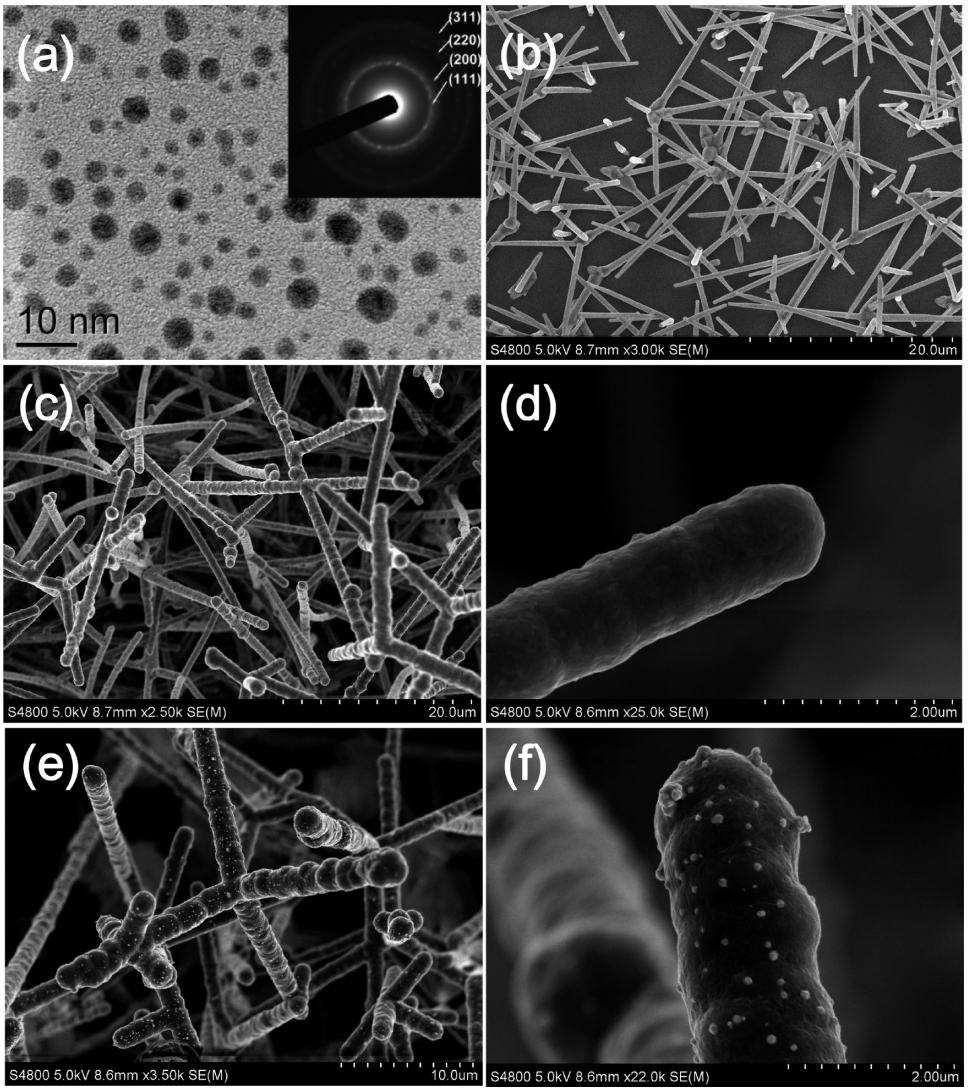

Figure 2. (a) TEM image of Au NPs. The inset is the corresponding SAED pattern. (b) SEM image of pure ZnO nanorods. (c) Low- and (d) high-magnification SEM images of V_2O_5@ZnO nanorods. (e) Low- and (f) high-magnification SEM images of Au-decorated V_2O_5@ZnO nanorods.

input flows were stopped, the furnace was cooled to room temperature, and the color of the substrate changed from light white to dark gray (Figure 1b). Subsequently, the dark-gray intermediate heteronanostructures were soaked in a Au NP suspension for 2 h (Figure 1c). Then, the Au-decorated intermediate products were removed and dried at 60 °C (Figure 1d). After a thermal oxidization process at 350 °C for 60 min, the color of the products changed from dark-gray to yellow, and the ternary photocatalyst of Au-decorated V_2O_5@ZnO nanorods was finally obtained. In addition, to investigate the effect of Au NPs on photocatalysis performance, another sample of V_2O_5@ZnO was also synthesized using the same method (excluding the soaking step) for comparison.

Characterization. The morphologies and sizes of the product were characterized by field-emission scanning electron microscopy (FESEM; JEOL JSM-4800F) and transmission electron microscopy (TEM; JEOL JEM-2100). The crystal structure was characterized by X-ray diffraction (XRD; Bruker D8 Advance diffractometer) using monochromatized Cu Kα radiation (λ = 1.5418 Å). UV−visible spectra were recorded with a UNICO-2802 ultraviolet−visible spectrophotometer. Photoluminescence (PL) spectra were measured on a JY LabRAM HR 800UV spectrometer.

Photocatalytic Measurements. Considering its strong adsorption to metal-oxide surfaces, well-defined optical absorption, and good resistance to light degradation, methylene blue (MB) was chosen to examine the photodegradation using the new catalyst. The maximum optical absorption of MB at 664 nm was used to monitor the concentration. The photocatalytic activities of pure ZnO, V_2O_5@ZnO, and Au-decorated V_2O_5@ZnO were evaluated in terms of the degradation of MB at room temperature under UV−vis light. The as-fabricated photocatalyst (0.03 g) was added to a cylindrical container containing 100 mL of MB aqueous solution (10 mg L^{-1}). Before irradiation, the solution was stirred in the dark for 30 min to ensure the establishment of equilibrium between adsorption and desorption. To minimize the effects of heating, the photoreactor was fixed in a glass jacket and cooled by flowing water. The solution was irradiated with a tungsten halogen lamp ($\lambda \geq 340$ nm), and the MB concentration was analyzed by a UV−vis spectrophotometer (UNICO 2802) every 30 min during a total irradiation time of 150 min. The photocatalytic measurements of the three photocatalysts (ZnO, V_2O_5@ZnO, and Au-decorated V_2O_5@ZnO) were performed in three independent experiments. Additionally, recycling experiments for Au-decorated V_2O_5@ZnO were performed for four cycles to test its durability. After each cycle, the catalyst was filtered and washed thoroughly with distilled water several times to remove residual dye impurities and then dried at 60 °C for the next test.

RESULTS AND DISCUSSION

Figure 2a shows a typical TEM image of Au NPs prepared by the citrate method. The morphologies of the Au NPs are

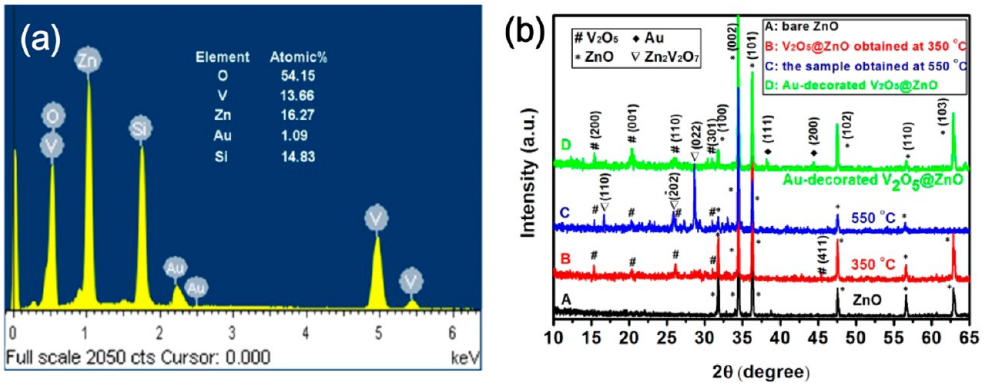

Figure 3. (a) EDX spectrum of Au-decorated V_2O_5@ZnO nanorods, along with semiquantitative elemental analysis results. (b) XRD spectra of (A) as-prepared pure ZnO (black), (B) V_2O_5@ZnO (red), and (D) Au-decorated V_2O_5@ZnO (green), as well as (C) a sample obtained at an oxidation temperature of 550 °C (blue).

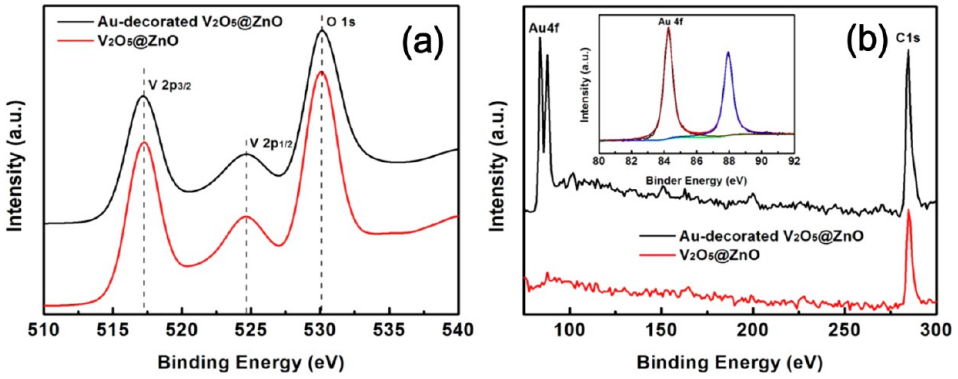

Figure 4. High-resolution XPS spectra of as-prepared V_2O_5@ZnO (red) and Au-decorated V_2O_5@ZnO (black): (a) V 2p and O 1s, (b) Au 4f and C 1s.

pseudospherical, and their size is less than 10 nm. The selected-area electron diffraction (SAED) pattern (inset of Figure 2a) shows four polycrystalline diffraction rings, corresponding to the (111), (200), (220), and (311) planes of Au. Figure 2b shows a typical SEM image of pure ZnO products synthesized by a thermal evaporation method. It can be seen that the products are composed of rodlike nanostructures with good quality and a smooth surface. The diameters of these ZnO rods are ~600 nm, and their lengths range from 10 to 25 μm. After application of the intermediate coating of V_2O_5 on the ZnO nanorods and oxidation in air at 350 °C, V_2O_5@ZnO heteronanorods were obtained. As shown in Figure 2c, the V_2O_5@ZnO nanorods still retained the initial shape of the ZnO nanorods; however, a rough and irregular surface can be clearly observed. In addition, the diameters of the V_2O_5@ZnO nanorods were markedly increased to ~900 nm (Figure 2d), indicating a film with a thickness of ~150 nm coated on the ZnO nanorods. For the ternary photocatalyst of Au-decorated V_2O_5@ZnO, the corresponding low- and high-magnification SEM images are shown in panels e and f, respectively, of Figure 2. Clearly, the morphology is very similar to that in Figure 2c,d, except that a large quantity of inlaid Au NPs is widely distributed in the surface (Figure 2e,f). To validate its composition, the Au-decorated V_2O_5@ZnO (Figure 2e,f) was investigated by means of energy-dispersive X-ray (EDX) spectroscopy. As shown in Figure 3a, V, Zn, O, and Au elements could be detected, confirming the components of Au, V_2O_5, and ZnO. The element Si should belong to the silicon substrate used in the synthesis process. Further semi-quantitative analysis showed that the atomic percentages of Au, V, Zn, and O were 1.09%, 13.66%, 16.27%, and 54.15%, respectively. Thus, the molar ratio of Au, ZnO, and V_2O_5 was calculated to be 1.09:16.27:6.83. The theoretical stoichiometric atomic proportion of O contained in ZnO and V_2O_5 was calculated to be 50.42%, which was slightly lower than the actual EDX result (54.15%) and should be attribute to the oxidation of the silicon substrate during the thermal oxidization process.

The purities and crystalline phases of the as-prepared samples were analyzed by X-ray diffraction (XRD). In the XRD patterns shown in Figure 3b, the curves for bare ZnO, V_2O_5@ZnO, and Au-decorated V_2O_5@ZnO are shown in black (A), red (B), and green (D), respectively. The XRD pattern of bare ZnO nanorods (Figure 3b, curve A) shows only peaks of wurtzite ZnO (JCPDS 36-1451). For the V_2O_5@ZnO nanorods obtained at 350 °C (Figure 3b, curve B), the XRD measurements verified that there was a new phase in addition to wurtzite ZnO that could be indexed to orthorhombic V_2O_5 (JCPDS 41-1426). When the oxidization temperature was increased to 550 °C, some other sharp diffraction peaks related to $Zn_2V_2O_7$ (110), ($\bar{2}$02), and (022) (JCPDS 38-0251) were observed in the XRD pattern (Figure 3b, curve C). Thus, the phase changes in the heteronanorods were quite sensitive to the oxidization temperature. To obtain pure V_2O_5@ZnO heteronanorods, the oxidation temperature should be controlled in an appropriate range during the annealing process. For the Au-decorated V_2O_5@ZnO sample, two characteristic peaks related to Au (111) and (200) (JCPDS 04-0784) were observed in the

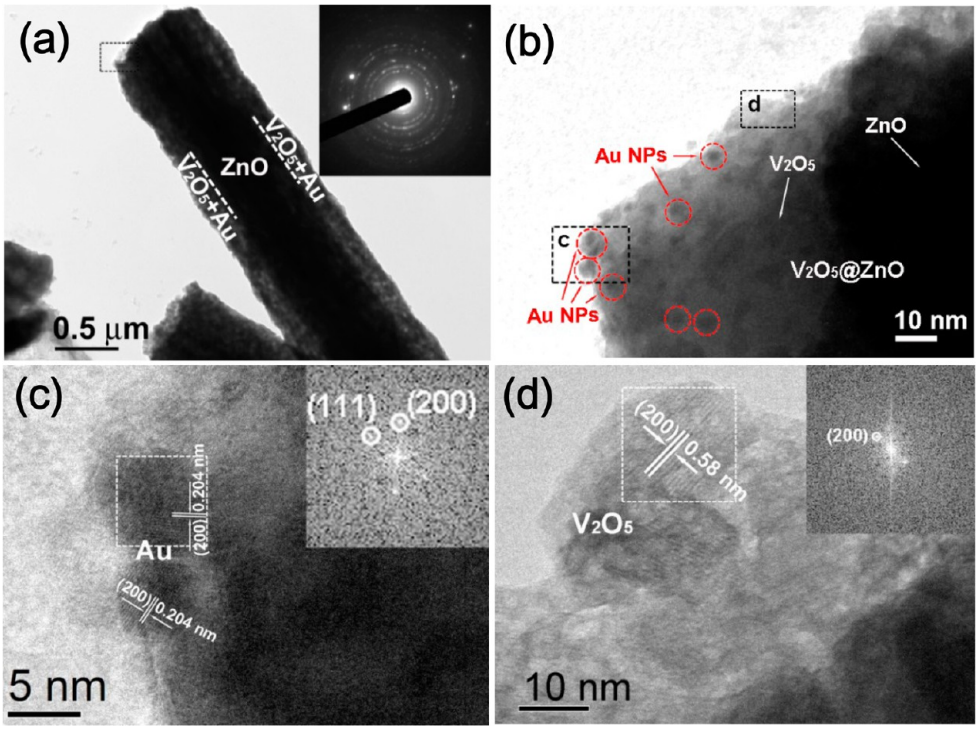

Figure 5. (a) Low-magnification TEM image of a single Au-decorated V_2O_5@ZnO nanorod (inset: corresponding SAED pattern). (b) Enlarged TEM image of the tip marked by the black rectangle in panel a. (c,d) Magnified HRTEM images from the regions labeled c and d in panel b (insets: corresponding fast Fourier transform (FFT) patterns of the regions marked by white squares).

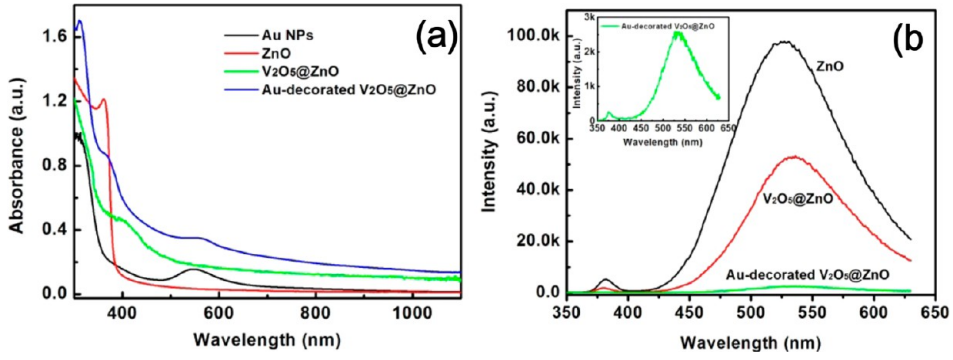

Figure 6. (a) UV−vis absorption spectra of Au NPs, bare ZnO, V_2O_5@ZnO, and Au-decorated V_2O_5@ZnO nanorods. (b) Photoluminescence spectra of pure ZnO, V_2O_5@ZnO, and Au-decorated V_2O_5@ZnO nanorods. Inset: Expanded photoluminescence spectrum of Au-decorated V_2O_5@ZnO nanorods.

diffraction pattern (Figure 3b, curve D), and all other diffraction peaks could be suitably indexed to orthorhombic V_2O_5 and wurtzite ZnO, revealing the high purity of the sample and the coexistence of Au, V_2O_5, and ZnO.

To further investigate the chemical state of the as-prepared V_2O_5@ZnO and Au-decorated V_2O_5@ZnO nanorods, X-ray photoelectron spectroscopy (XPS) was carried out, and the corresponding spectra are shown in Figure 4a,b. The binding energies obtained in the XPS analysis were corrected for specimen charging by referencing the C 1s to 284.8 eV. It was verified that both vanadium and oxygen were found in the two samples (Figure 4a), and extra peaks indexed to Au were observed for the Au-decorated V_2O_5@ZnO sample (Figure 4b). The XPS peaks of V and O were observed at the same points for the two samples (Figure 4a), revealing the same major composition for the two samples' shells. The V 2p core level spectra display two representative peaks located at 517.3 and 524.6 eV, corresponding to the V $2p_{3/2}$ and V $2p_{1/2}$ states, respectively, of V^{5+}. An O 1s peak located at 530.1 eV is also observed in Figure 4a, corresponding to the O 1s state of O^{2-}. In Figure 4b, the XPS signal for Au-decorated V_2O_5@ZnO shows only the spin−orbit splitting of the Au 4f (84.3 eV) and Au 0 (87.9 eV) states, without any indication of ionic species, confirming the presence of Au particles inlaid in the V_2O_5 shell.

Figure 5a shows a low-magnification TEM image of a single Au-decorated V_2O_5@ZnO nanorod, where the ZnO core with a diameter of ∼600 nm was coated by a V_2O_5 film with a thickness of ∼160 nm. In the SAED pattern shown in the inset of Figure 5a, two sets of diffraction patterns can be observed: The bright and clear diffraction spots belong to the single-crystal ZnO core, and the regular polycrystalline diffraction rings can be attributed to the polycrystalline V_2O_5 shell. Note that the polycrystalline diffraction rings from Au NPs were weak compared to those of V_2O_5 and ZnO because of the small

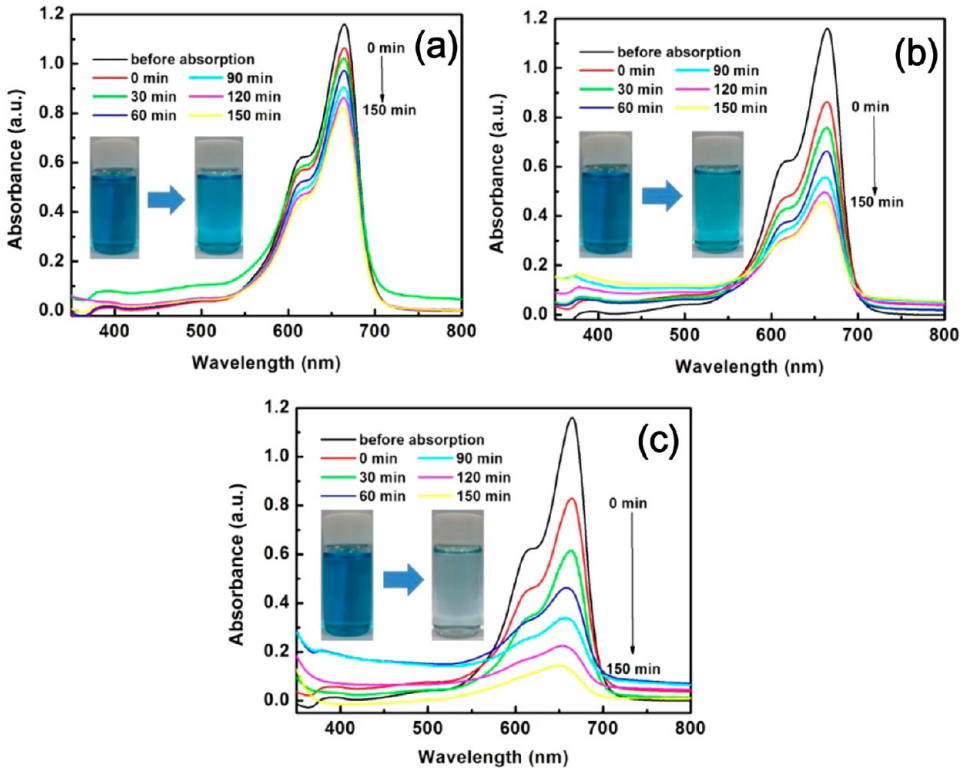

Figure 7. UV−vis absorption spectra and photographs of MB solutions in the presence of (a) pure ZnO, (b) V_2O_5@ZnO, and (c) Au-decorated V_2O_5@ZnO nanorods.

portion in the local selective nanoscale zone, so they were not recorded here. In the enlarged TEM image of the rod tip (Figure 5b), the contrast between the Au NPs (dark) and the V_2O_5 film (bright) confirms the inlay of Au NPs. Here, the introduced Au NPs appear black, and the V_2O_5 film is bright, because Au has a higher mass−thickness contrast. In addition, it is obvious that the Au NPs are widely distributed in the V_2O_5 shell and that their size is less than 10 nm, agreeing with the results in Figure 2a. The high-resolution (HR) TEM images shown in Figure 5c,d were recorded from different regions as marked in Figure 5b: The region labeled c (magnified in Figure 5c) exhibits a lattice spacing of 0.204 nm, which is consistent with the (200) plane of Au; the region labeled d (magnified in Figure 5d) exhibits a lattice spacing of 0.58 nm, which is consistent with the (200) plane of V_2O_5. These results confirm the coexistence of Au NPs and V_2O_5 in the heteronanorods.

Figure 6a shows UV−vis absorption spectra of the Au NPs, bare ZnO, V_2O_5@ZnO, and Au-decorated V_2O_5@ZnO. The absorption of the bare ZnO nanorods shows a sharp edge at ~380 nm, which is related to its band-edge absorption, as the band gap of ZnO is about 3.3 eV. For the as-prepared V_2O_5@ZnO nanorods, the absorption edge becomes ambiguous compared to that of pure ZnO. The average absorption for UV light weakens slightly, whereas the absorption in the visible range strengthens greatly, confirming enhanced absorption in the visible range. In addition, pure Au NPs exhibit an LPSR peak at 549 nm in the visible region because of a collective oscillation of the free electrons. When Au NPs were introduced onto V_2O_5@ZnO nanorods, an increased absorption intensity and a significant red shift of the LSPR peak were observed, as shown in Figure 6a. The LSPR peak of the Au NPs shifted from 549 nm to the longer wavelength of 562 nm because of an increase in the local refractive index of the dielectric environment surrounding the Au NPs by the V_2O_5 coating on one side.[34,45]

Moreover, the interface charge-separation and recombination properties of as-prepared samples were investigated by photoluminescence (PL) emission spectroscopy. Figure 6b compares the PL emission spectra of bare ZnO, V_2O_5@ZnO , and Au-decorated V_2O_5@ZnO. Pure ZnO exhibited a narrow UV emission with a peak at 381 nm and a broad green emission with a peak at 525 nm. The UV emission band was due to the near-band-edge transition, and the green emission originated from defect emissions in the ZnO crystals. After application of the polycrystalline V_2O_5 film, the green emission peak shifted from 525 to 534 nm because of the relatively narrow band gap (2.2 eV) of V_2O_5, and the PL emission intensity was found to be notably weakened compared to that of pure ZnO. For the Au-decorated V_2O_5@ZnO sample, the PL emission bands were very similar to those of V_2O_5@ZnO; however, the PL emission intensity was further weakened, and the emission bands almost disappeared, as shown in Figure 6b. It has been established that charge-carrier transfer between different parts of composites usually results in the weakening of PL emission bands. In our case, because of the staggered band offset, the photogenerated electrons and holes were separated and confined mainly in different components. This would decrease the recombination rate of electrons and holes and consequently weaken the PL intensity.

The photocatalytic activity of the Au-decorated V_2O_5@ZnO nanorods was evaluated in the photodegradation of MB dye in water under UV−vis light irradiation. The characteristic absorption of MB at 664 nm was used to monitor the photocatalytic degradation process. As depicted in Figure 7c, the main absorption peaks of MB decreased gradually as irradiation proceeded and almost vanished after 150 min.

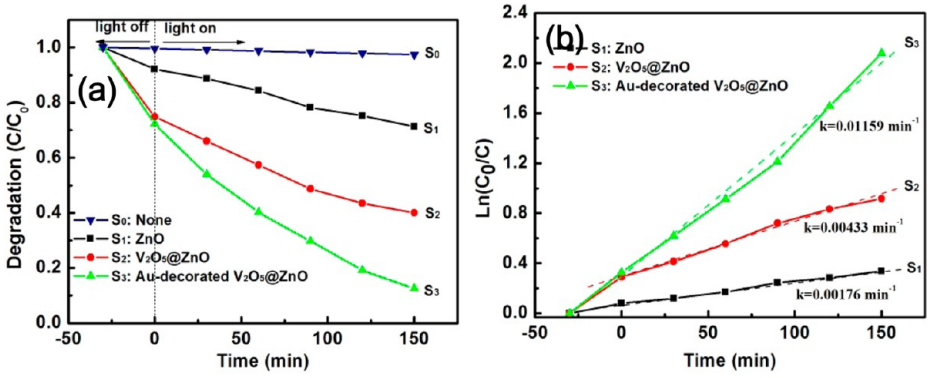

Figure 8. (a) Decrease (C/C_0) and (b) natural logarithm $[\ln(C_0/C)]$ of the normalized concentration vs irradiation time for MB solutions containing different photocatalysts: S_1, ZnO nanorods; S_2, V_2O_5@ZnO nanorods; S_3, Au-decorated V_2O_5@ZnO nanorods. The dashed lines in panel b represent the linear fitting results corresponding to the three different photocatalysts.

Correspondingly, the color of the solution became lighter and lighter until the solution became completely translucent in the end. These observations reveal that the chromophoric structure of MB was gradually decomposed during the reaction process. For comparison, bare ZnO and V_2O_5@ZnO were also employed as reference catalysts, and the corresponding absorption spectra are shown in panels a and b, respectively, of Figure 7. Obviously, the MB solution containing V_2O_5@ZnO exhibited a much higher rate of decrease of the MB absorption peak than that containing pure ZnO nanorods, but the value was much lower than that of the Au-decorated V_2O_5@ZnO, revealing that the photocatalysis performance was improved by introducing V_2O_5 and Au NPs onto ZnO.

The dependencies of the degradation efficiency on irradiation time for the samples are presented in Figure 8a. The degradation efficiency is defined as C/C_0, where C and C_0 correspond to the remaining concentration and the initial concentration of MB, respectively. After ZnO nanorods had been added to the MB solution and the solution had been kept in the dark, a small decrease in concentration (S_1 in Figure 8a) was observed because of the adsorption of MB molecules onto ZnO. In contrast, dramatic decreases in the MB concentration were observed when the other two samples (V_2O_5@ZnO and Au-decorated V_2O_5@ZnO) were employed (S_2 and S_3 in Figure 8a), exhibiting higher adsorption abilities. The high adsorption ability should be mainly attributed to the strong adsorption of the V_2O_5 polycrystalline shell and is beneficial in improving photocatalytic performance.[17] According to Figure 8a, Au-decorated V_2O_5@ZnO nanorods showed the strongest photocatalytic activity under UV−vis light irradiation for 150 min, and the photocatalytic activities of the three samples followed the order Au-decorated V_2O_5@ZnO nanorods > V_2O_5@ZnO nanorods > ZnO nanorods. After 150 min of reaction, the degradation efficiencies of the three samples were calculated to be ∼22.6%, ∼46.5%, and ∼82.6%, respectively. In addition, a plot of $\ln(C_0/C)$ versus time is shown in Figure 8b, indicating that MB photodegradation followed pseudo-first-order kinetics on these catalysts. According to the Langmuir−Hinshelwood model, the linear relationship of $\ln(C_0/C)$ versus time can be described as $\ln(C_0/C) = kt + A$, where the slope k represents the photodegradation rate. Thus, the constant photodegradation rates were calculated and are included in Figure 8b. In a series of samples, Au-decorated V_2O_5@ZnO nanorods showed the highest photodegradation rate of 0.01159 min^{-1}; a high photodegradation rate (0.00433 min^{-1}) for V_2O_5@ZnO nanorods was also obtained, although the value was lower than for Au-decorated V_2O_5@ZnO, whereas the photodegradation rate of bare ZnO nanorods was the lowest with a value of 0.00176 min^{-1}. For comparison, the same photodegradation experiment in the absence of photocatalyst was carried out, and no appreciable degradation of MB was observed after 150 min of irradiation (curve S_0, blue line in Figure 8a). Therefore, it was concluded that the greatly enhanced photodegradation activity of Au-decorated V_2O_5@ZnO indeed originated from the introduction of V_2O_5 and Au NPs.

To clarify whether the ZnO/V_2O_5 interface plays an essential role in elevating the photodegradation activity, another photodegradation measurement using pure V_2O_5 nanowires was also performed and compared with the results for bare ZnO and V_2O_5@ZnO (see Supporting Information, section S-1). Clearly, V_2O_5@ZnO nanorods showed a higher photodegradation activity than either bare ZnO or pure V_2O_5. Thus, the coupling of V_2O_5 with ZnO can elevate the photodegradation activity, and the ZnO/V_2O_5 interface plays a crucial role in the MB photodegradation reaction. Combined with above UV−vis absorption spectra and PL and analysis, it can be demonstrated that the enhanced visible-light absorption and the decreased carrier recombination rate mainly lead to the greatly enhanced photodegradation activity.

In addition to photocatalytic activity, the stability of a photocatalyst is another important issue for its practical application. Therefore, cycling experiments were performed to evaluate the decreased concentration of MB under UV−vis light irradiation, and all processes and parameters were kept unchanged. As shown in Figure 9, Au-decorated V_2O_5@ZnO used for the degradation of MB showed a slight decline after four cycles of experimental tests: ∼81.8% of the original MB was degraded after the fourth run, whereas the extent of degradation was 87.5% for the first run, confirming the stability of our Au-decorated V_2O_5@ZnO plasmonic photocatalysts during the photocatalytic process.

Based on the above experimental results and previous studies,[34,45,46] the enhanced photodegradation activities of V_2O_5@ZnO and Au-decorated V_2O_5@ZnO can be attributed to synergistic effects and specific charge-transfer kinetics. Herein, the photocatalytic mechanism can be understood as described below. The work function of V_2O_5 shell was studied by ultraviolet photoelectron spectroscopy (UPS), and its value was determmined to be 5.57 eV (see Supporting Information, section S-2), in agreement with recent Kelvin probe (KP) results.[47] In previous studies, the work functions of ZnO and

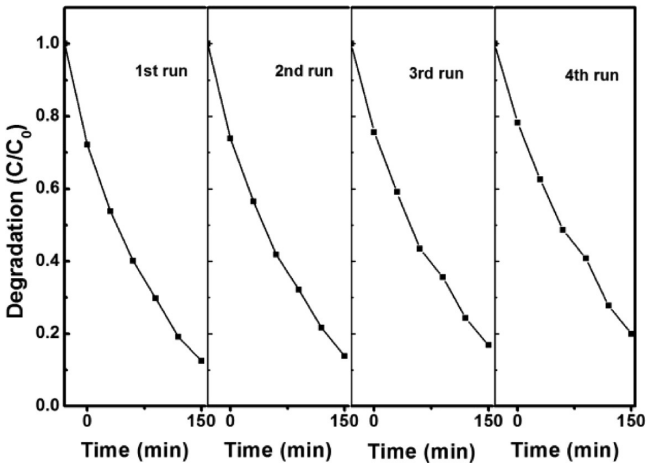

Figure 9. Cycling runs in the photodegradation of MB in the presence of Au-decorated V_2O_5@ZnO nanorods under UV-vis light irradiation.

Au crystals were reported to be 5.3 and 5.1 eV, respectively,[48,49] indicating that ZnO crystal has a Fermi level (E_F) lower than that of Au metal but higher than that of V_2O_5 (Figure 10a). Only UV light can excite electron−hole pairs from bare ZnO nanorods, and the recombination rate is too high, so the photodegradation efficiency is the lowest. For V_2O_5@ZnO, both ZnO and V_2O_5 have essentially the same Fermi energy level at the interface, so a staggered band offset is formed near the interface, as shown in Figure 10b. When V_2O_5@ZnO nanorods are irradiated with UV−vis light, electrons in V_2O_5 and ZnO are excited by visible and UV light, respectively, so more carrier pairs can be photogenerated and elevate the photocatalytic ability. Meanwhile, the photogenerated electrons can transfer into the conduction band. Because the conduction and valence bands of V_2O_5 lie below the energy band of ZnO (Figure 10b), the electrons excited from ZnO can easily cross the interface and transfer to the conduction band of V_2O_5. Likewise, the holes excited from V_2O_5 can easily cross the interface and transfer to the valence band of ZnO. Thus, the photogenerated electrons and holes can be separated efficiently at the interface, which is beneficial in hindering the recombination of electron and hole pairs and, ultimately, elevating the photocatalytic ability. For Au-decorated V_2O_5@ZnO, the carrier-transfer mechanism between ZnO and V_2O_5 is similar to that for V_2O_5@ZnO, where the excited holes are also transferred into the valence band from V_2O_5 to ZnO. However, gold NPs in the ternary photocatalyst also play a vital role in the photocatalytic reaction. The LSPR effect introduced by the Au NPs is an important factor in achieving an enhanced photodegradation ability. The coupling of V_2O_5 and Au NPs forms a noncentrosymmetric (Janus) morphology. In many previous studies, it has been verified that the noncentrosymmetric coupling of metal nanoparticles with dielectric oxides can generate extremely strong local electric near-fields.[34,45] In our experiments, excitation of the LSPR takes place under visible-light irradiation, resulting in the generation of plasmonic near-fields that are strongly localized close to the Au−V_2O_5 interface. In this region, the surface plasmon excitations are converted into electron−hole pairs through optical transitions,

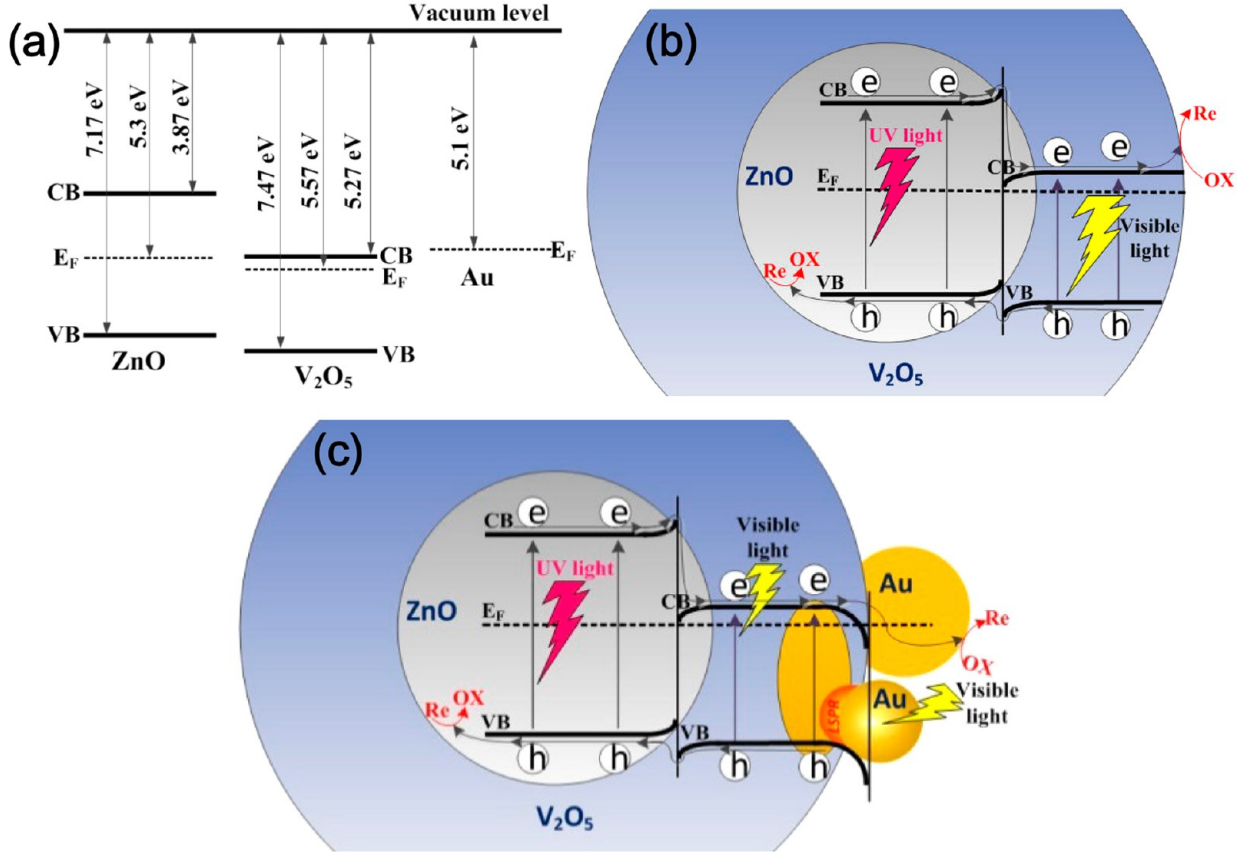

Figure 10. (a) Schematic diagram of the band configurations for ZnO, V_2O_5 and Au crystals. (b,c) Schematic diagrams of the band configurations and charge-carrier transfer processes in (b) V_2O_5@ZnO and (c) Au-decorated V_2O_5@ZnO nanorods.

and more electron−hole pairs are excited from V_2O_5. Because the energy level of the V_2O_5 conduction band is higher than the Fermi level of the Au NPs (Figure 10c), the excited electrons transfer from the V_2O_5 conduction band into the Au NPs. Finally, a transfer route for the excited electrons from ZnO to V_2O_5 and then to Au NPs is formed in the ternary photocatalyst. The Au nanoparticles act as a sink for the photogenerated electrons, preventing them from recombining with holes in the valence band, thus facilitating the separation of photogenerated electrons and holes and enhancing the photocatalytic activity.

CONCLUSIONS

In summary, a ternary plasmonic photocatalyst of Au-decorated V_2O_5@ZnO heteronanorods was successfully synthesized by an innovative method. Three-dimensional ZnO templates were first synthesized by a thermal evaporation route, and the final ternary heteronanostructures were obtained after coating, Au NP decoration, and thermal oxidization processes. An SEM investigation revealed that the morphology of the final ternary heterophotocatalyst was determined by the morphology of the three-dimensional ZnO template, where a large quantity of Au NPs were inlaid in the V_2O_5 shell. The uniform coating of V_2O_5 and the high-quality contacts with Au NPs and ZnO cores can enlarge the light-absorption region, benefit the efficient spatial separation of charge, and minimize the recombination rate of photogenerated carriers. Thus, an enhanced visible absorption and a significantly decreased PL emission intensity compared to those of pure ZnO and V_2O_5@ZnO were observed in the UV−vis absorption and PL spectra, respectively. In the application of the photocatalyst for MB dye photodegradation, the ternary photocatalyst of Au-decorated V_2O_5@ZnO exhibited a markedly enhanced photocatalytic activity, showing an increased photodegradation rate of 0.01159 min^{-1}, which is about 3 and 7 times the rates of pure ZnO and V_2O_5@ZnO, respectively. The photocatalytic mechanism analysis revealed that the coupling of V_2O_5 and Au plays an essential role in improving the photocatalytic activity, owing to the enlarged light absorption region, the strong localization of plasmonic near-field effects, and the effective electron−hole separation at interfaces caused by the staggered band offset.

ASSOCIATED CONTENT

Supporting Information

Photodegradation measurement of pure V_2O_5 nanowires and UPS analysis of V_2O_5 film. This material is available free of charge via the Internet at http://pubs.acs.org.

AUTHOR INFORMATION

Corresponding Author

*Tel.: +86 21 54345198; Fax: +86 21 54345119. E-mail: yk5188@263.net.

Notes

The authors declare no competing financial interest.

ACKNOWLEDGMENTS

The authors acknowledge financial support from the NSF of China (Grants 61204018, 61274014, 61474043, 61371111, 61371112, and 81371663), the NSF of Jiangsu Province (Grant BK20141239), the Innovation Research Project of the Shanghai Education Commission (Grant 13zz033), the Education Committee of Jiangsu Province (Grant 14KJB510029), the Six Top Talents of Jiangsu Province (Grant XCL-013), The Doctoral Scientific Research Funds of Nantong University (13B23 and 13B25), and the Project of Key Laboratory of Polar Materials and Devices (Grant KFKT2014003).

REFERENCES

(1) Irie, H.; Watanabe, Y.; Hashimoto, K. Nitrogen-Concentration Dependence on Photocatalytic Activity of $TiO_{2-x}N_x$ Powders. *J. Phys. Chem. B* **2003**, *107*, 5483−5486.

(2) Sakthivel, S.; Neppolian, B.; Shankar, M. V.; Arabindoo, B.; Palanichamy, M.; Murugesan, V. Solar Photocatalytic Degradation of Azo Dye: Comparison of Photocatalytic Efficiency of ZnO and TiO_2. *Sol. Energy Mater. Sol. Cells* **2003**, *77*, 65−82.

(3) Vinodgopal, K.; Kamat, P. V. Enhanced Rates of Photocatalytic Degradation of an Azo Dye Using SnO_2/TiO_2 Coupled Semiconductor Thin Films. *Environ. Sci. Technol.* **1995**, *29*, 841−845.

(4) Li, L.; Chu, Y.; Liu, Y.; Dong, L. Template-Free Synthesis and Photocatalytic Properties of Novel, Fe_2O_3 Hollow Spheres. *J. Phys. Chem. C* **2007**, *111*, 2123−2127.

(5) Chen, D.; Ye, J. Hierarchical WO_3 Hollow Shells: Dendrite, Sphere, Dumbbell, and Their Photocatalytic Properties. *Adv. Funct. Mater.* **2008**, *18*, 1922−1928.

(6) Kim, Y.; Park, K. Y.; Jang, D. M.; Song, Y. M.; Kim, H. S.; Cho, Y. J.; Myung, Y.; Park, J. Synthesis of Au−Cu_2S Core−Shell Nanocrystals and Their Photocatalytic and Electrocatalytic Activity. *J. Phys. Chem. C* **2010**, *114*, 22141−22146.

(7) Li, Q.; Guo, B.; Yu, J.; Ran, J.; Zhang, B.; Yan, H.; Gong, J. R. Highly Efficient Visible-Light-Driven Photocatalytic Hydrogen Production of CdS-Cluster-Decorated Graphene Nanosheets. *J. Am. Chem. Soc.* **2011**, *133*, 10878−10884.

(8) Hu, J. S.; Ren, L. L.; Guo, Y. G.; Liang, H. P.; Cao, A. M.; Wan, L. J.; Bai, C. L. Mass Production and High Photocatalytic Activity of ZnS Nanoporous Nanoparticles. *Angew. Chem., Int. Ed.* **2005**, *44*, 1269−1273.

(9) Zhang, K.-L.; Liu, C.-M.; Huang, F.-Q.; Zheng, C.; Wang, W.-D. Study of the Electronic Structure and Photocatalytic Activity of the BiOCl Photocatalyst. *Appl. Catal. B: Environ.* **2006**, *68*, 125−129.

(10) Zhang, J.; Shi, F.; Lin, J.; Chen, D.; Gao, J.; Huang, Z.; Ding, X.; Tang, C. Self-Assembled 3-D Architectures of BiOBr as a Visible Light-Driven Photocatalyst. *Chem. Mater.* **2008**, *20*, 2937−2941.

(11) Xia, J.; Yin, S.; Li, H.; Xu, H.; Yan, Y.; Zhang, Q. Self-Assembly and Enhanced Photocatalytic Properties of BiOI Hollow Microspheres via a Reactable Ionic Liquid. *Langmuir* **2011**, *27*, 1200−1206.

(12) Djurisic, A. B.; Chen, X.; Leung, Y. H.; Man Ching Ng, A. ZnO Nanostructures: Growth, Properties and Applications. *J. Mater. Chem.* **2012**, *22*, 6526−6535.

(13) Yu, Z. B.; Xie, Y. P.; Liu, G.; Lu, G. Q.; Ma, X. L.; Cheng, H.-M. Self-Assembled CdS/Au/ZnO Heterostructure Induced by Surface Polar Charges for Efficient Photocatalytic Hydrogen Evolution. *J. Mater. Chem. A* **2013**, *1*, 2773−2776.

(14) Huang, X.; Shang, L.; Chen, S.; Xia, J.; Qi, X.; Wang, X.; Zhang, T.; Meng, X.-M. Type-II ZnO Nanorod−SnO_2 Nanoparticle Heterostructures: Characterization of Structural, Optical and Photocatalytic Properties. *Nanoscale* **2013**, *5*, 3828−3833.

(15) Roy, P.; Periasamy, A. P.; Liang, C.-T.; Chang, H.-T. Synthesis of Graphene−ZnO−Au Nanocomposites for Efficient Photocatalytic Reduction of Nitrobenzene. *Environ. Sci. Technol.* **2013**, *47*, 6688−6695.

(16) Wang, Y.; Su, Y. R.; Qiao, L.; Liu, L. X.; Su, Q.; Zhu, C. Q.; Liu, X. Q. Synthesis of One-Dimensional TiO_2/V_2O_5 Branched Heterostructures and Their Visible Light Photocatalytic Activity towards Rhodamine B. *Nanotechnology* **2011**, *22*, 225702.

(17) Zhu, Q.; Wang, W.-S.; Lin, L.; Gao, G.-Q.; Guo, H.-L.; Du, H.; Xu, A.-W. Facile Synthesis of the Novel Ag_3VO_4/AgBr/Ag Plasmonic Photocatalyst with Enhanced Photocatalytic Activity and Stability. *J. Phys. Chem. C* **2013**, *117*, 5894−5900.

(18) Liu, S.; Li, C.; Yu, J.; Xiang, Q. Improved Visible-Light Photocatalytic Activity of Porous Carbon Self-Doped ZnO Nanosheet-Assembled Flowers. *CrystEngComm* **2011**, *13*, 2533−2541.
(19) Mapa, M.; Gopinath, C. S. Combustion Synthesis of Triangular and Multifunctional $ZnO_{1-x}N_x$ ($x \leq 0.15$) Materials. *Chem. Mater.* **2008**, *21*, 351−359.
(20) Deng, Z. W.; Chen, M.; Gu, G. X.; Wu, L. M. A Facile Method to Fabricate ZnO Hollow Spheres and Their Photocatalytic Property. *J. Phys. Chem. B* **2008**, *112*, 16−22.
(21) Wang, L. N.; Zheng, Y. Y.; Li, X. Y.; Dong, W. J.; Tang, W. H.; Chen, B. Y.; Li, C. R.; Li, X.; Zhang, T. R.; Xu, W. Nanostructured Porous ZnO Film with Enhanced Photocatalytic Activity. *Thin Solid Films* **2011**, *519*, 5673−5678.
(22) Huang, Y.-C.; Chang, S.-Y.; Lin, C.-F.; Tseng, W. J. Synthesis of ZnO Nanorod Grafted TiO_2 Nanotube 3-D Arrayed Heterostructure as Supporting Platform for Nanoparticle Deposition. *J. Mater. Chem.* **2011**, *21*, 14056−14061.
(23) Jung, S.; Yong, K. Fabrication of CuO−ZnO Nanowires on a Stainless Steel Mesh for Highly Efficient Photocatalytic Applications. *Chem. Commun.* **2011**, *47*, 2643−2645.
(24) Zou, C. W.; Rao, Y. F.; Alyamani, A.; Chu, W.; Chen, M. J.; Patterson, D. A.; Emanuelsson, E. A. C.; Gao, W. Heterogeneous Lollipop-Like V_2O_5/ZnO Array: A Promising Composite Nanostructure for Visible Light Photocatalysis. *Langmuir* **2010**, *26*, 11615−11620.
(25) Pei, C. C.; Leung, W. W.-F. Enhanced Photocatalytic Activity of Electrospun TiO_2/ZnO Nanofibers with Optimal Anatase/Rutile Ratio. *Catal. Commun.* **2013**, *37*, 100−104.
(26) Guo, S.; Han, S.; Mao, H.; Dong, S.; Wu, C.; Jia, L.; Chi, B.; Pu, J.; Li, J. Structurally Controlled ZnO/TiO_2 Heterostructures as Efficient Photocatalysts for Hydrogen Generation from Water without Noble Metals: The Role of Microporous Amorphous/Crystalline Composite Structure. *J. Power Sources* **2014**, *245*, 979−985.
(27) Liu, Y.; Shi, J.; Peng, Q.; Li, Y. CuO Quantum-Dot-Sensitized Mesoporous ZnO for Visible-Light Photocatalysis. *Chem.—Eur. J.* **2013**, *19*, 4319−4326.
(28) Simon, Q.; Barreca, D.; Gasparotto, A.; Maccato, C.; Montini, T.; Gombac, V.; Fornasiero, P.; Lebedev, O. I.; Turner, S.; Van Tendeloo, G. Vertically Oriented CuO/ZnO Nanorod Arrays: From Plasma-Assisted Synthesis to Photocatalytic H_2 Production. *J. Mater. Chem.* **2012**, *22*, 11739−11747.
(29) Chouhan, N.; Yeh, C. L.; Hu, S. F.; Liu, R. S.; Chang, W. S.; Chen, K. H. Photocatalytic CdSe Qds-Decorated ZnO Nanotubes: An Effective Photoelectrode for Splitting Water. *Chem. Commun.* **2011**, *47*, 3493−3495.
(30) Glaspell, G.; Hassan; Elzatahry, A.; Fuoco, L.; Radwan, N. R. E.; El-Shall, M. S. Nanocatalysis on Tailored Shape Supports: Au and Pd Nanoparticles Supported on MgO Nanocubes and ZnO Nanobelts. *J. Phys. Chem. B* **2006**, *110*, 21387−21393.
(31) Herring, N. P.; AbouZeid, K.; Mohamed, M. B.; Pinsk, J.; El-Shall, M. S. Formation Mechanisms of Gold−Zinc Oxide Hexagonal Nanopyramids by Heterogeneous Nucleation Using Microwave Synthesis. *Langmuir* **2011**, *27*, 15146−15154.
(32) Tahir, M. N.; Natalio, F.; Cambaz, M. A.; Panthofer, M.; Branscheid, R.; Kolb, U.; Tremel, W. Controlled Synthesis of Linear and Branched Au@ZnO Hybrid Nanocrystals and Their Photocatalytic Properties. *Nanoscale* **2013**, *5*, 9944−9949.
(33) Chen, Y.; Zeng, D.; Zhang, K.; Lu, A.; Wang, L.; Peng, D.-L. Au−ZnO Hybrid Nanoflowers, Nanomultipods and Nanopyramids: One-Pot Reaction Synthesis and Photocatalytic Properties. *Nanoscale* **2014**, *6*, 874−881.
(34) Wu, W.; Liao, L.; Zhang, S.; Zhou, J.; Xiao, X.; Ren, F.; Sun, L.; Dai, Z.; Jiang, C. Non-Centrosymmetric Au−SnO_2 Hybrid Nanostructures with Strong Localization of Plasmonic for Enhanced Photocatalysis Application. *Nanoscale* **2013**, *5*, 5628−5636.
(35) Wen, Y.; Liu, B.; Zeng, W.; Wang, Y. Plasmonic Photocatalysis Properties of Au Nanoparticles Precipitated Anatase/Rutile Mixed TiO_2 Nanotubes. *Nanoscale* **2013**, *5*, 9739−9746.
(36) Wang, H.; You, T.; Shi, W.; Li, J.; Guo, L. Au/TiO_2/Au as a Plasmonic Coupling Photocatalyst. *J. Phys. Chem. C* **2012**, *116*, 6490−6494.
(37) Tanaka, A.; Fuku, K.; Nishi, T.; Hashimoto, K.; Kominami, H. Functionalization of Au/TiO_2 Plasmonic Photocatalysts with Pd by Formation of a Core−Shell Structure for Effective Dechlorination of Chlorobenzene under Irradiation of Visible Light. *J. Phys. Chem. C* **2013**, *117*, 16983−16989.
(38) Martha, S.; Das, D. P.; Biswal, N.; Parida, K. M. Facile Synthesis of Visible Light Responsive V_2O_5/N,S-TiO_2 Composite Photocatalyst: Enhanced Hydrogen Production and Phenol Degradation. *J. Mater. Chem.* **2012**, *22*, 10695−10703.
(39) Su, Q.; Zhang, J.; Wang, Y.; Yu, M.; Zhu, C.; Lan, W.; Liu, X. Effect of the Morphology of V_2O_5/TiO_2 Nanoheterostructures on the Visible Light Photocatalytic Activity. *J. Phys. Chem. Solids* **2013**, *74*, 1475−1481.
(40) Shahid, M.; Shakir, I.; Yang, S.-J.; Kang, D. J. Facile Synthesis of Core−Shell SnO_2/V_2O_5 Nanowires and Their Efficient Photocatalytic Property. *Mater. Chem. Phys.* **2010**, *124*, 619−622.
(41) Wang, Y.; Zhang, J.; Liu, L.; Zhu, C.; Liu, X.; Su, Q. Visible Light Photocatalysis of V_2O_5/TiO_2 Nanoheterostructures Prepared via Electrospinning. *Mater. Lett.* **2012**, *75*, 95−98.
(42) El-Sharkawy, E. A.; Soliman, A. Y.; Al-Amer, K. M. Comparative Study for the Removal of Methylene Blue via Adsorption and Photocatalytic Degradation. *J. Colloid Interface Sci.* **2007**, *310*, 498−508.
(43) Yin, H.; Yu, K.; Peng, H.; Zhang, Z.; Huang, R.; Travas-Sejdic, J.; Zhu, Z. Porous V_2O_5 Micro/Nano-Tubes: Synthesis via a CVD Route, Single-Tube-Based Humidity Sensor and Improved Li-Ion Storage Properties. *J. Mater. Chem.* **2012**, *22*, 5013−5019.
(44) Yin, H.; Song, C.; Wang, Y.; Li, S.; Zeng, M.; Zhang, Z.; Zhu, Z.; Yu, K. Influence of Morphologies and Pseudocapacitive Contributions for Charge Storage in V_2O_5 Micro/Nano-Structures. *Electrochim. Acta* **2013**, *111*, 762−770.
(45) Seh, Z. W.; Liu, S.; Low, M.; Zhang, S.-Y.; Liu, Z.; Mlayah, A.; Han, M.-Y. Janus Au−TiO_2 Photocatalysts with Strong Localization of Plasmonic Near-Fields for Efficient Visible-Light Hydrogen Generation. *Adv. Mater.* **2012**, *24*, 2310−2314.
(46) You, H.; Liu, R.; Liang, C.; Yang, S.; Wang, F.; Lu, X.; Ding, B. Gold Nanoparticle Doped Hollow SnO_2 Supersymmetric Nanostructures for Improved Photocatalysis. *J. Mater. Chem. A* **2013**, *1*, 4097−4104.
(47) Zilberberg, K.; Trost, S.; Schmidt, H.; Riedl, T. Solution Processed Vanadium Pentoxide as Charge Extraction Layer for Organic Solar Cells. *Adv. Energy Mater.* **2011**, *1*, 377−381.
(48) Zhai, T.; Liu, H.; Li, H.; Fang, X.; Liao, M.; Li, L.; Zhou, H.; Koide, Y.; Bando, Y.; Golberg, D. Centimeter-Long V_2O_5 Nanowires: From Synthesis to Field-Emission, Electrochemical, Electrical Transport, and Photoconductive Properties. *Adv. Mater.* **2010**, *22*, 2547−2552.
(49) Zhang, Z.; Meng, G. W.; Xu, Q. L.; Hu, Y. M.; Wu, Q.; Hu, Z. Aligned ZnO Nanorods with Tunable Size and Field Emission on Native Si Substrate Achieved via Simple Electrodeposition. *J. Phys. Chem. C* **2010**, *114*, 189−193.